PCCP

Accepted Manuscript

ROYAL SOCIETY OF CHEMISTRY

www.rsc.org/pccp

The influence of fibrous carbon envelope on the formation of Co-Fe nanoparticles for durable electrocatalytic oxygen evolution reaction

Beomgyun Jeong,[a,+] Dongyoon Shin,[a,+] Jae Kwang Lee,[b] Dae Han Kim,[c] Young Dok Kim,[c] Jaeyoung Lee[a,b*]

[a]*Electrochemical Reaction and Technology Laboratory (ERTL), School of Environmental Science and Engineering, GIST, Gwangju 500-712, Republic of Korea*
[b]*Ertl Center for Electrochemistry and Catalysis, RISE, GIST, Gwangju 500-712, Republic of Korea*
[c]*Department of Chemistry, Sungkyunkwan University, Suwon 440-746, Republic of Korea*

Abstract

Co oxides are known to be active and stable alternative anode electrocatalyst possibly replacing the best performing but the most expensive Ir and Ru oxides in an alkaline water electrolysis. Of late, there are researches on Co oxides loaded on various carbon supports as a way to outperform Ir or Ru catalysts by improving the utilization efficiency. In this study, we introduce Co and Fe nanoparticles embedded carbon nanofibers (CoFe-CNFs), fabricated through electrospinning and pyrolysis of a polymer mixed with Co and Fe precursors, a facile route for simultaneously making Co and Fe nanoparticles and the carbon support stably accommodating them. We demonstrate the potential of CoFe-CNF as active and stable electrocatalysts for oxygen evolution reaction (OER) in an alkaline media. We conducted detailed physico-chemical characterizations to elucidate the effect of CNF on the OER activity and stability of CoFe-CNFs. It is suggested that CNF is a medium in which OER-active CoFe alloy nanoparticles are formed homogeneously, and that carbon layers surrounding the nanoparticles are beneficial to the stability of CoFe-CNFs in OER.

*Corresponding Author. E-mail: jaeyoung@gist.ac.kr (J. Lee)

[+] These authors contributed equally to this work.

1. Introduction

Oxygen evolution reaction (OER) has been a holy-grail study for a long time in electrochemistry field because it is involved in major electrochemical processes as a rate determining reaction such as electrometallurgy, water electrolysis, regenerative fuel cells and metal-air battery.[1] Along with the fundamental studies to understand the electrocatalysis in OER,[2,3] an electrode lowering the necessary polarization for making the same level of oxygen evolving electrical current has been searched and some of materials show excellent OER activity approaching to the fundamental activation energy limit such as Beer's dimensionally stable anode (DSA) comprising Ru and Ir oxides developed in 1969.[4,5] It has been enough to be used in specialized processes for obtaining high-purity metal, hydrogen, and oxygen. However, as needs for storing renewable energy and also batteries with higher energy density increase, finding a more cost-efficient OER electrocatalyst having similar performance and stability to the expensive Ru and Ir oxide based electrocatalyst is becoming another challenge for making metal-air battery and regenerative fuel cell as a viable option for storing renewable energy.

In practical point of view, it is extremely difficult to find such alternative catalysts replacing the Ru and Ir oxides in acidic media, in which non-noble metals are chemically unstable and they show the worse OER activity. In contrast, Fe, Co, and Ni (iron triad) oxides with amorphous or spinel structure are chemically stable in alkaline media and they show relatively comparable OER performance to Ru and Ir oxides.[1,6–9] Thus, there are studies on improving the performance of iron triad elements based electrocatalysts by introducing novel carbon supports such as carbon nanotubes, and graphene,[10–13] and studies to find out the optimum oxidation state or surface oxide structure of Fe, Co and Ni based electrocatalysts.[6,14] These optimally controlled oxidation state and appropriate carbon support resulted in similar

activity toward OER and also superior stability in alkaline media. In the synthesis of these electrocatalysts, metal salts dissolved and nano-carbons dispersed in water or organic solvent having high dielectric constant and heated around 150-200 ^{o}C for several hours to make a metal oxide loaded on the carbon nanomaterials. Although the metal oxide loading process on the nanocarbon support is relatively facile, synthesis of carbon nanotube and graphene, and adjustment of the graphitic surface to easily accept metal precursor through wet process are not easy as the metal loading process.

We introduced Co and Fe modified electrospun carbon nanofibers (CoFe-CNFs) as a facile one-step synthesis of electrocatalysts toward oxygen reduction reaction (ORR).[15,16] In ORR, the metal particles embedded in the carbon nanofibers (CNF) facilitate the formation of ORR active sites and graphitization, moreover, they contribute to improve the conductivity of the CNF network through percolating conduction. In this work, we extended application of the developed CoFe-CNFs to OER from the expectation that the metal particles embedded in CNFs can act as direct electrocatalysts toward OER.[15,17,18] The metal particles formed inside the carbon nanofibers are uniform because they are under homogeneous temperature and environment condition in high temperature heat-treatment process. The carbon layer surrounding the metal particles provides stronger interaction to the CNF support and it prevents chemical degradation of the metal surface for better stability. Thus, CoFe-CNFs would be able to show a potential as stable, controllable, and cost-effective OER electrocatalysts as well as bi-functional oxygen electrocatalysts applicable to regenerative fuel cells and metal-air batteries. In this study, we tested the OER performance including activity and stability of CoFe-CNFs by the comparison with Ir electrocatalysts, and we investigated the effect of CNF in CoFe-CNF during OER.

2. Experimental methods

The metal-embedded CNFs (Me-CNFs) were prepared by electrospinning the metal precursor containing polymer to polymeric nanofiber web and subsequent high temperature heat-treatments. For preparing metal precursor containing polymer, 4 g polyacrylonitrile (PAN) solution were dissolved in 36 g N,N-dimethylformamide at 60-80 ^{o}C for around 3 hrs. After complete mixing PAN in N,N-dimethylformamide, the polymer solution was mixed with the metal precursors, Co(II) nitrate hexahydrate ($Co(NO_3)_2$•$6H_2O$) and Fe(III) nitrate nonahydrate ($Fe(NO_3)_3$•$9H_2O$). The total weight of metal precursors were the same to 1.2 g in all metal precursor containing PAN (Me-PAN), and a weight ratio of Co and Fe precursor was 1 to 1 in case of CoFe-PAN solution. The resultant weight ratio of the precursor is PAN:DMF=1:9 and Co or Fe metal precursor:(PAN+DMF)=3:100. For electrospinning of the Me-PAN solution, it was supplied at a flow rate of 5 ml h^{-1} for 6 h via 5 multi-nozzle equipped in a syringe pump. A high voltage of +12 kV was applied to the syringe needles and -12 kV to the drum collector, which are located 15 cm apart from each other. All processes were performed at room temperature (~ 25 ^{o}C) under a controlled relative humidity of 30 %. In the stabilizing heat treatment of Me-CNF, the electrospun Me-PAN fiber web was heated in air environment at a ramping rate 1 ^{o}C min^{-1} up to 280 ^{o}C then waited for an hour at the temperature. Then, the environment has been changed by flowing N_2 at a flow rate of 200 ml min^{-1} and the temperature is controlled to 1000 ^{o}C at a ramping rate of 5 ^{o}C min^{-1} and maintained the temperature for 1 hr in order to carbonize the stabilized Me-PAN fiber web. Finally, we obtain the metal containing carbon nanofibers (Me-CNFs), i.e. Co-CNFs, Fe-CNFs, and CoFe-CNFs. The prepared Me-CNFs were grinded with mortar for electrochemical experiments with rotating disk electrode (RDE). For preparation of the intensively pulverized CoFe-CNFs, 0.2 g of CoFe-CNFs was mixed with 20 g of germanium

oxide balls having 2 mm diameter and the CoFe-CNFs was ball-milled at 500 rpm for 160 min with 10 min idle time and 30 min process time.

Electrochemical properties and OER activity of the synthesized Co-CNFs, Fe-CNFs, and CoFe-CNFs catalysts were evaluated using a three electrode cell connected to a potentiostat/galvanostat (Biologic, VSP). A smooth Pt wire was used as the counter electrode and Hg/HgO as the reference. All potentials initially measured versus the Hg/HgO electrode immersed in 1 M NaOH were converted to a RHE scale by adding 0.9083 V to the potentials.

We prepared a catalyst ink by dispersing 25 mg synthesized catalysts in a mixture of 25 μl of 10 wt% Nafion solution (Sigma-Aldrich), 2.5 ml D.I. water and 2.5 ml isopropyl alcohol. After the catalyst ink was ultrasonicated for 30 min, a 10 μl aliquot of the suspension was dropped onto glassy carbon disk electrode (0.2475 cm^2) using a micropipette, so that the amount of the catalysts on the electrode is 200 $\mu g/cm^2$. The reference Ir catalyst ink was prepared by ultrasonically dispersing for 30 min 5 mg of Ir black (99.9% trace metals basis, Sigma-Aldrich) in 5 ml solution containing N-propyl alcohol and deionized water, 1:1 by volume and same amount of the suspension was dropped onto glassy carbon disk electrode.

Cyclic voltammograms (CVs) were obtained in an aqueous solution of 0.1 M potassium hydroxide (KOH) as electrolyte that was saturated by ultrapure N_2 bubbling at room temperature. The scan rate was 50 mV s^{-1} and the potential range was from 0.6 V to -1.2 V versus (vs.) Hg/HgO. The OER activities of synthesized catalysts were measured with RDE at rotating rate of 1600 rpm while nitrogen was constantly bubbled at a flow rate of 10 ml/min; the potential was scanned from 0 V to 1.5 V vs. Hg/HgO at a scan rate of 100 mV s^{-1}. Chronoamperometry was also performed to obtain long term stability of catalysts at 0.9 V vs. Hg/HgO electrode.

The structural changes in the bulk crystallinity depending on the sort of metal were

investigated using X-ray diffraction (XRD; Rigaku Miniflex II) equipped with Cu Kα (λ = 0.15406 nm) X-ray source. Morphological properties and quantitative elemental compositions of the catalysts were investigated through scanning transmission/transmission electron microscope (STEM/TEM; Philips TECNAI F20) and energy-dispersive X-ray spectroscopy (EDS) analysis in Korea Basic Science Institute (KBSI), Gwangju center. The X-ray photoelectron spectroscopy (XPS) was performed to investigate surface functionality and oxidation state of metal in an ultrahigh vacuum (UHV) chamber with a base pressure $\leq 2.0 \times 10^{-10}$ Torr and a concentric hemispherical analyzer (CHA; PHOIBOS-Has 3500, SPECS). All XPS spectra were obtained at room temperature using the Mg Kα-line (1253.6 eV) as photon source and the binding energy of the measured peaks is calibrated with respect to C 1s peak position (284.6 eV). The specific surface area and pore size distribution of Me-CNF were also detemined by N_2 adsorption using the BET method and BJH method respectively at 77 K with an automatic gas adsorption-desorption apparatus (Belsorp-max, Japan).

3. Results and discussion

The TEM images of Me-CNFs show similar morphology for different types of metals, the most metal nanoparticles are homogeneously embedded in CNFs (Fig. S1). The size of metal particles ranged around 10-50 nm as shown in Fig. S1, and the diameter of CNFs is approximately in the range from 100-500 nm from our previous studies.[15,16,18] For CoFe-CNFs, Co particles are homogeneously distributed together with Fe particles as seen Fig. 1a-d. From the EDS elemental composition shown in Table 1, slightly larger amount of Co is detected in CoFe-CNFs, which is expected from the molar ratio of Co and Fe calculated from the precursors' molecular weights. The relative amount of metal particles in Me-CNFs measured with point EDS

analysis is around 13 wt%. However, according to the ICP-AES analysis conducted in the previous study, approximately 20 wt% of metal is included in Me-CNFs, which is more representative and conclusive than EDS elemental ratio for several strands of Me-CNF. In the EDS line mapping result for a metal particle in CoFe-CNFs (Fig. 1f), the molar ratio of Co:Fe=1:1 is observed, which is implying the formation of CoFe alloy.

This implication corresponds with the XRD result showing CoFe as the main crystal component (Fig. 2), and the slightly excess Co seems to comprise CoC_x. The crystal structure of Me-CNFs shows quite different features according to the types of metal precursors used in the synthesis of Me-CNFs. In the XRD result of Co-CNFs, metallic Co is the main crystal component. In contrast, for Fe-CNFs, Fe carbide (Fe_3C) is the main component rather than forming metallic Fe separated from the carbon medium. The crystallite size of embedded metal particles in Fe-CNFs estimated from the Debye-Scherrer equation is around 13 nm, smaller than Co-CNFs and CoFe-CNFs having around 24-25 nm size. The smaller particle size of Fe particles is likely to be related to the formation of Fe carbide where Fe atoms are well-dispersed in carbon medium. In the case of CoFe-CNFs, Fe atoms look to form alloys with Co atoms, so that Fe atoms are less dispersed in carbon to form smaller Fe carbide particles. In the previous study that we conducted with Co-CNFs,[16] the FWHM of graphite peak (002) in XRD of Co-CNF becomes narrower than those of Fe-CNFs and CoFe-CNFs. Co atoms mixed with polymer facilitate the graphitization of carbon fibers when it is under heat-treatment, which can be beneficial to electrical conductivity.[19]

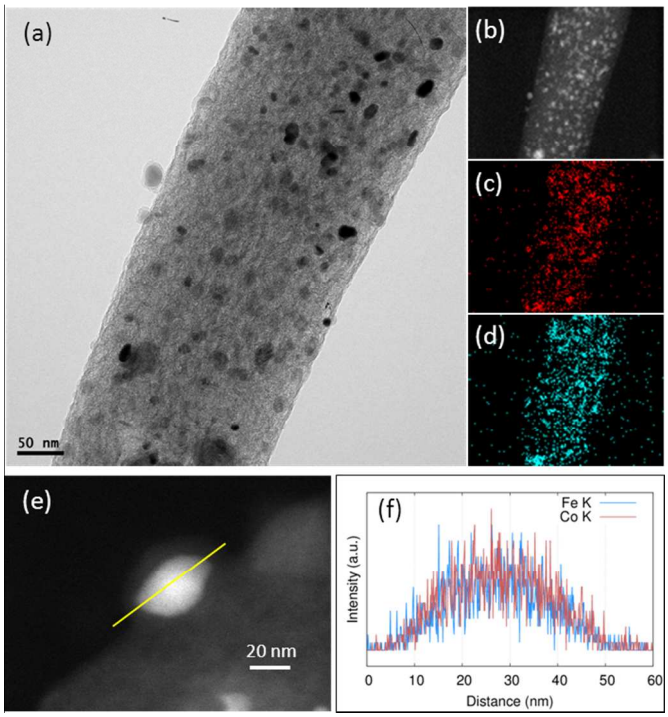

Fig. 1. (a) TEM image, (b) STEM image of CoFe-CNFs, EDS maps for (c) Fe and (d) Co, respectively, in the same STEM image. Magnified STEM images and linear EDS profiles of carbon layer enclosed metal particles with (e) and (f) roughly Co:Fe=1:1 ratio.

Table 1. EDS elemental analysis of CoFe-CNFs

Element	wt %	at %
C	81.4	92.2
N	0	0
O	5.5	4.7
Fe	5.7	1.4
Co	7.3	1.7

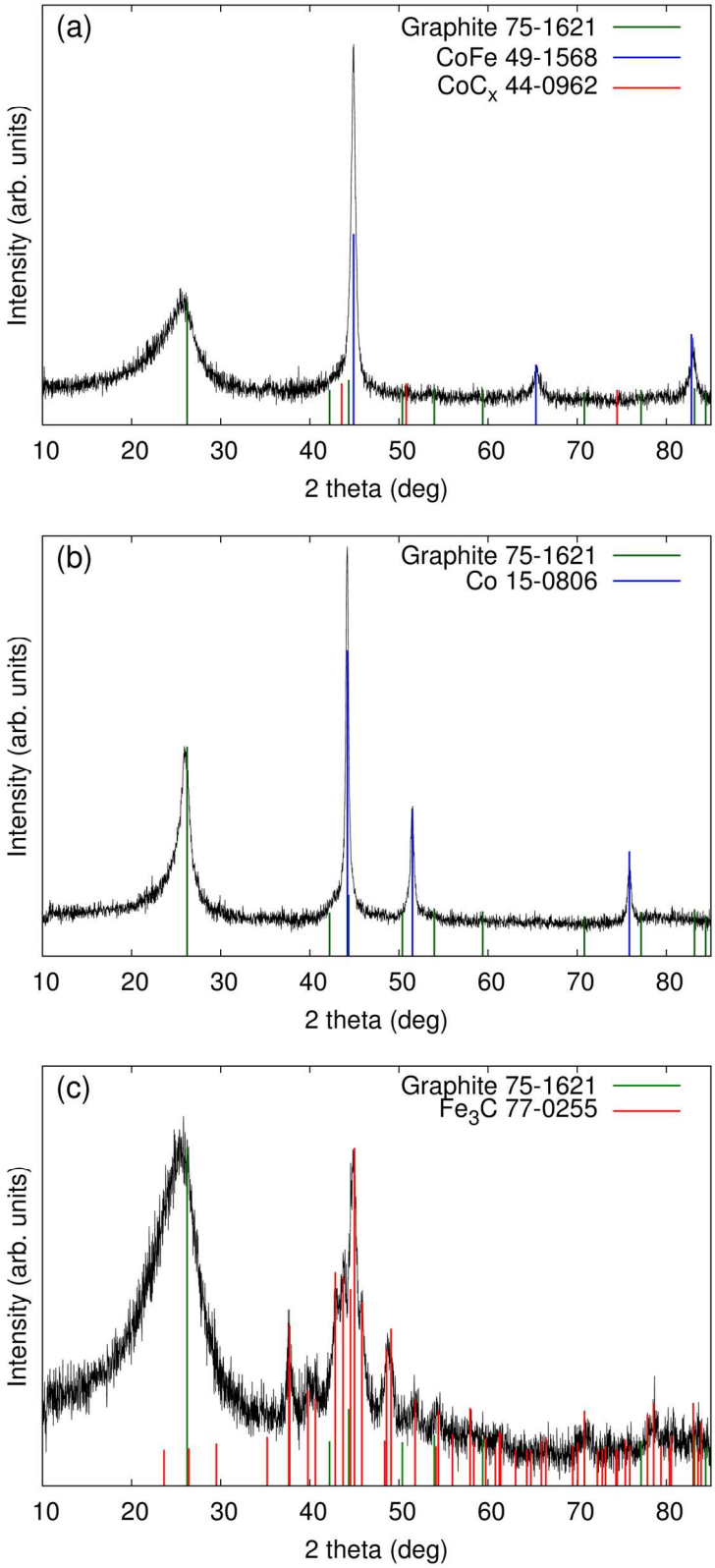

Fig. 2. XRD results of (a) CoFe-CNFs, (b) Co-CNFs, and (c) Fe-CNFs.

Table 2. Approximate size of embedded particles in Me-CNFs calculated from the XRD result

	FWHM	Peak Location	Lower size limit	FWHM of graphite (002) peak
CoFe-CNF	0.55°	44.9°	24 nm	3.7°
Co-CNF	0.32°	44.2°	25 nm	3.4°
Fe-CNF	1.01°	44.9°	13 nm	1.6°

The cyclic voltammograms (CVs) of Me-CNFs (Fig. 3) show characteristic redox peaks closely related to metal components and surface oxide species although most of metal particles visible in the TEM images are buried inside CNFs. It suggests that the electrolyte is penetrable through the carbon layers surrounding the metal nanoparticles, which are important OER active sites. Fe-CNFs shows broad peaks appearing at around -0.06 V on the cathodic scan and 0.28 V on the anodic scan, which is characteristic feature of Fe(II)/Fe(III) redox surface reaction.[14,20,21] Co-CNFs shows Co(II)/Co(III) redox peaks in the range of 0.95-1.25 V corresponding to CoO or $Co(OH)_2$ → Co_3O_4, Co_2O_3 or CoOOH, and Co(0)/Co(II) redox peaks corresponding to Co → $Co(OH)_2$, CoO, or $CoO{\cdot}OH_{aq}$ located at around 0.30 V on the anodic scan and 0.40 V on the cathodic scan.[14,22] CoFe-CNFs has an intermediate CV shape between Co-CNFs and Fe-CNFs; CV shape of CoFe-CNFs in the lower potential range is similar to Fe-CNFs and there is seemingly Co-related redox peak in the higher potential range. However, the Co redox peak of CoFe-CNFs looks different to Co-CNFs, the Co redox peaks centered at 1.07 V becomes substantially suppressed and a new Co redox peak is slightly appeared at around 1.30 V also identified in CV measurement for Co oxides film in Doyle et al.'s study.[14] This Co redox peak

appeared at 1.30 V vs. RHE is clearly observable in ball-milled CoFe-CNFs likely from the more exposed Co and Fe metal surface. Integrated charge and equivalent capacitance of these metal-modified CNFs is in the range roughly between 50-100 F/g, which is difficult to achieve with electric double layer of carbon material having BET surface area less than 500 m^2/g (Fig. S3).

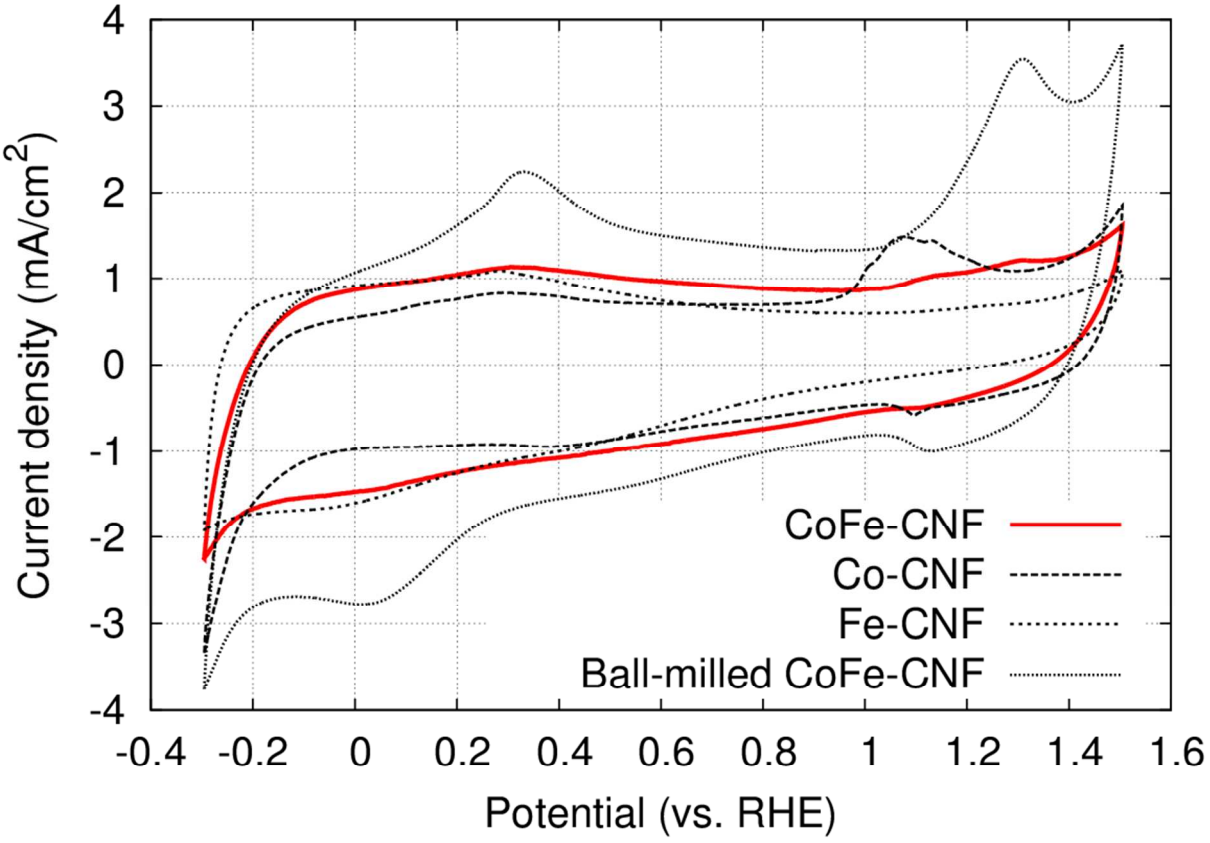

Fig. 3. Cyclic voltammograms of CoFe-CNFs, Co-CNFs, Fe-CNFs, and ball-milled CoFe-CNFs in 0.1 M KOH aqueous solution at a scan rate of 50 mV/s.

We tested OER activity of Me-CNFs through 50 scans of cyclic voltammetry in the range 0.9-2.4 V vs. RHE in 0.1 M KOH aqueous solution using RDE at rotating speed of 1600 rpm to exclude oxygen bubbles blocking the coated catalyst surface (Fig. S2). We compared the OER activity of Me-CNFs (200 μg/cm^2 loading on GC) at the fiftieth scan with Ir black catalyst with the same metal loading amount of 40 μg/cm^2 considering that the metal content in Me-CNFs is

about 20 wt% as investigated with ICP-AES analysis. CoFe-CNFs displays fairly comparable OER current to Ir black catalyst at around over 2.0 V vs. RHE (Fig. 4) and maintained its OER performance over 50 scans event though it went through highly anodic potential up to 2.4 V vs. RHE in every scan (Fig. 5). Co-CNFs also shows similar tendency in OER stability but with lower OER activity than CoFe-CNFs with the same metal loading amount. Thus, Me-CNFs including Co metal like Co-CNFs and CoFe-CNFs might have advantageous property in OER stability. Note that Fe-CNFs shows poor OER activity and stability but CoFe-CNFs shows enhanced activity and stability even comparing to Co-CNFs with double Co metal amount. The improvement of OER activity of CoFe is in accordance with the result reported from Smith *et al*., in which CoFe oxide layer demonstrates significantly low Tafel slope close to 40 mV dec^{-1} and 0.25 V of overpotential at j=0.5 mA cm^{-2}.[8,9] Ball-milled CoFe-CNFs shows the more enhanced metal redox peaks in CV results representing the more exposed metal surface on the ball-milled CoFe-CNFs, and the higher OER activity than CoFe-CNFs in the potential range over 1.75 V, implying the disadvantage of the carbon layers around the metal particles in mass transport.

However, CoFe-CNFs shows similar OER activity at potentials below 1.75 V, and it is relatively more stable than the ball-milled CoFe-CNFs in OER. Thus, the carbon layers seem to provide a protective layer preventing possible detachment or dissolution of catalyst particle from the CNF support so that CoFe-CNFs have an improved stability without compromising the OER activity performance within a certain range of potential although the metallic nanoparticles themselves do not have such stability in harsh condition. The concept of enveloping the catalyst surface with thin carbon layer is reported in the research papers on ORR, and the patent documents on bi-functional OER/ORR electrocatalysts.[23–25] In this study, however, we could achieve the configuration beneficial to the catalytic stability by simply electrospinning and

carbonizing the mixture of metal and polymer precursors. Moreover, the formation of the optimum carbon layer for protecting the catalyst surface seems to depend on the nature of the enclosed metal particles. We also conducted chronoamperometry (CA) to evaluate the durability of CoFe-CNFs catalysts with the same metal amount of Ir black for comparison at 1.8 V vs. RHE (Fig. 6). The durability order shown in the CA result is the same to the tendency of cyclic durability result in Fig. 5, CoFe-CNFs > ball-milled CoFe-CNFs > Ir black. Especially, CoFe-CNFs suffered essentially little degradation in OER activity during the measurement time. Furthermore, we did additional experiments to confirm that the carbon layers around metal particles act protective layer for blocking the oxidation of metal (Fig. S4, S5). The Co oxidation state does not change before and after OER experiment and the metal particles are still well dispersed and do not agglomerate. Even though the peak intensity at around 288 eV (C=O) slightly increases in C 1s XPS spectra, it is not related to carbon corrosion which can significantly affect to the dimensional stability of the catalytic electrode. There is no indication of carbon corrosion such as substantial development of sp^3 bonding (C-C) or C-O functional group larger than sp^2 bonding (C=C). Therefore, we can conclude that carbon layer is fairly stable and it can act as a sacrificial layer to prevent oxidation of metal particles during OER.

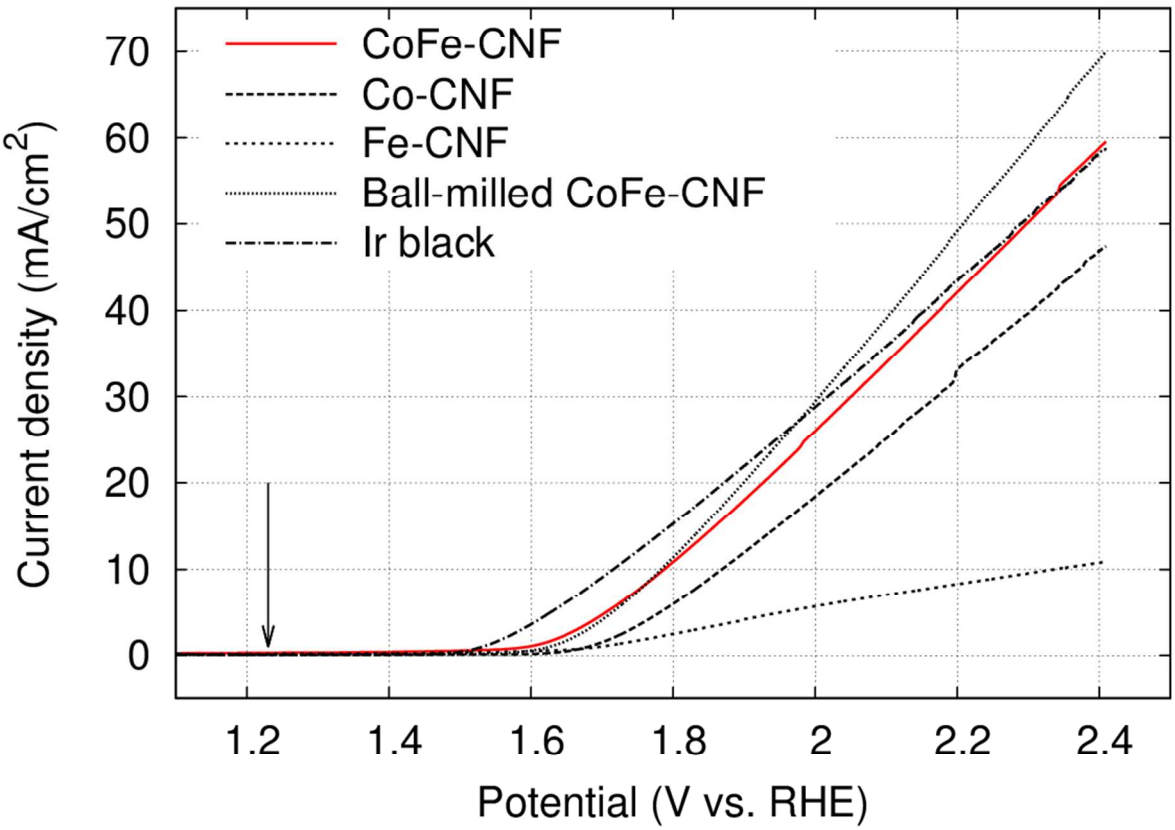

Fig. 4. OER activity of CoFe-CNFs, Co-CNFs, Fe-CNFs, ball-milled CoFe-CNFs, and Ir black. The metal loading amount of Me-CNFs and Ir black on GC is the same to 40 ug/cm^2. The arrow mark in this figure indicates the equilibrium potential of ORR/OER.

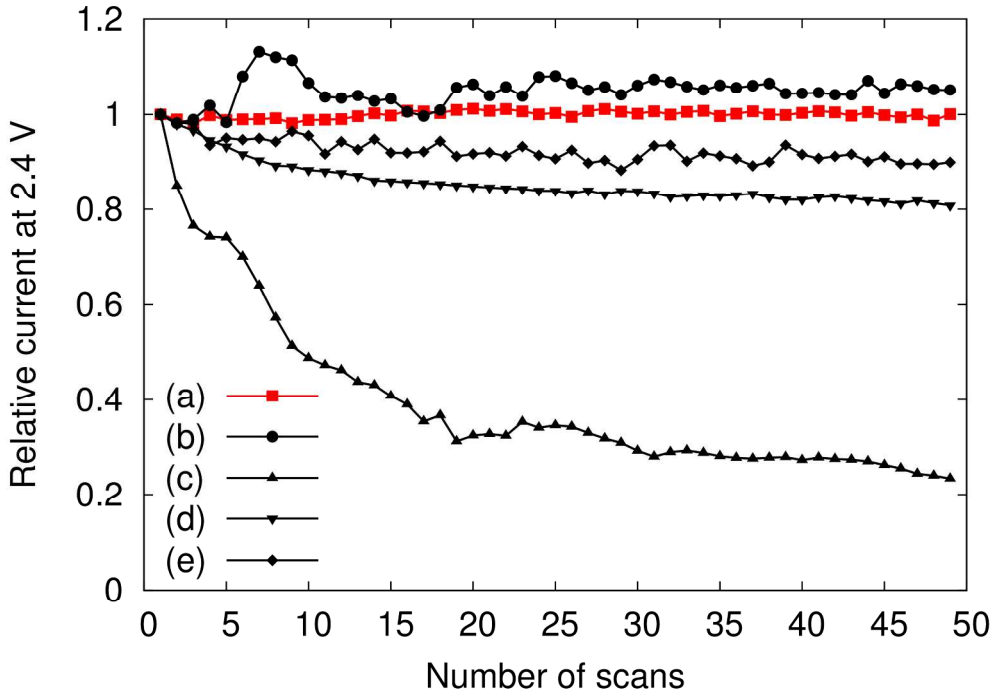

Fig. 5. Relative activity change according to number of scans of (a) CoFe-CNFs, (b) Co-CNFs, (c) Fe-CNFs, (d) ball-milled CoFe-CNFs, and (e) Ir black.

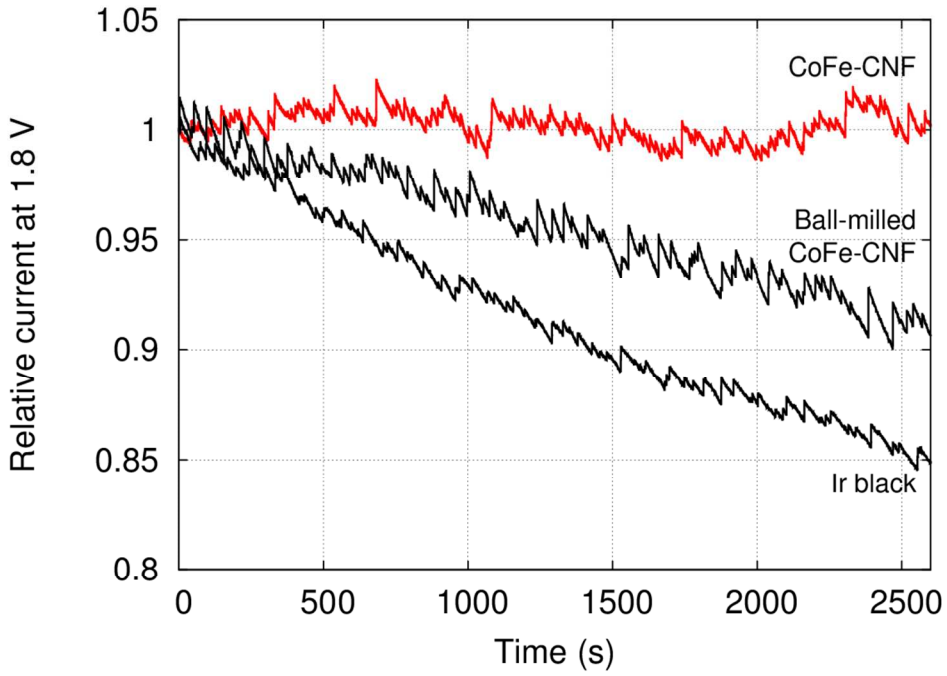

Fig. 6. Chronoamperometry for CoFe-CNFs, ball-milled CoFe-CNFs, and Ir black.

Like other XPS results measured in C 1s, N 1s, and O 1s regions (Fig. S6), XPS of CoFe-CNF and Co-CNF measured in Co 2p region do not show significant difference in shape of the profile; the intensity is slightly different due to the higher Co metal content in Co-CNFs than CoFe-CNFs (Fig. 7a and b). The XPS peak shape of Co-CNFs and CoFe-CNFs resembles to the known XPS results of Co(II) oxides, CoO and $Co(OH)_2$.[26,27] Although CoO and $Co(OH)_2$ show very similar profile of XPS peak, XPS peak of CoO in Co $2p_{1/2}$ region has a slight shoulder at binding energy of 794.5 eV, which is also quite clearly seen in the XPS of the ball-milled CoFe-CNFs having more exposed metal particles. The oxidation state of Co surface observed in XPS explains CVs of CoFe-CNFs and Co-CNFs having Co(II)/Co(III) redox peak dominantly. However, unlike similar Co 2p XPS profile between CoFe-CNFs and Co-CNFs in terms of binding energy shift or change in sub-peak distribution, the potential location and the shape of Co(II)/Co(III) peak in CV are different to each other. Considering great difference in analyzable depth of XPS and CV, the electrochemically influential catalytic sites related to OER activity seem to reside mainly inside CNFs. This result is due to the synthesis process of metal nanoparticles; metal precursors are homogeneously mixed with polymer precursor, then metal particles formed together when the polymer becomes carbonized at a high temperature. Then the generated metal nanoparticles are distributed mostly inside CNFs rather than exposed out to the surface of CNFs. XPS has been a standard and powerful technique for investigating the physicochemical property of conventional catalysts, in which metal nanoparticles dispersed on the support surface. However, for Me-CNFs having the metal nanoparticles with the carbon envelopes more than several nm thick, a surface analysis method with more analyzable depth such as CV would be a more reasonable choice for investigating the surface property of the electrocatalysts.

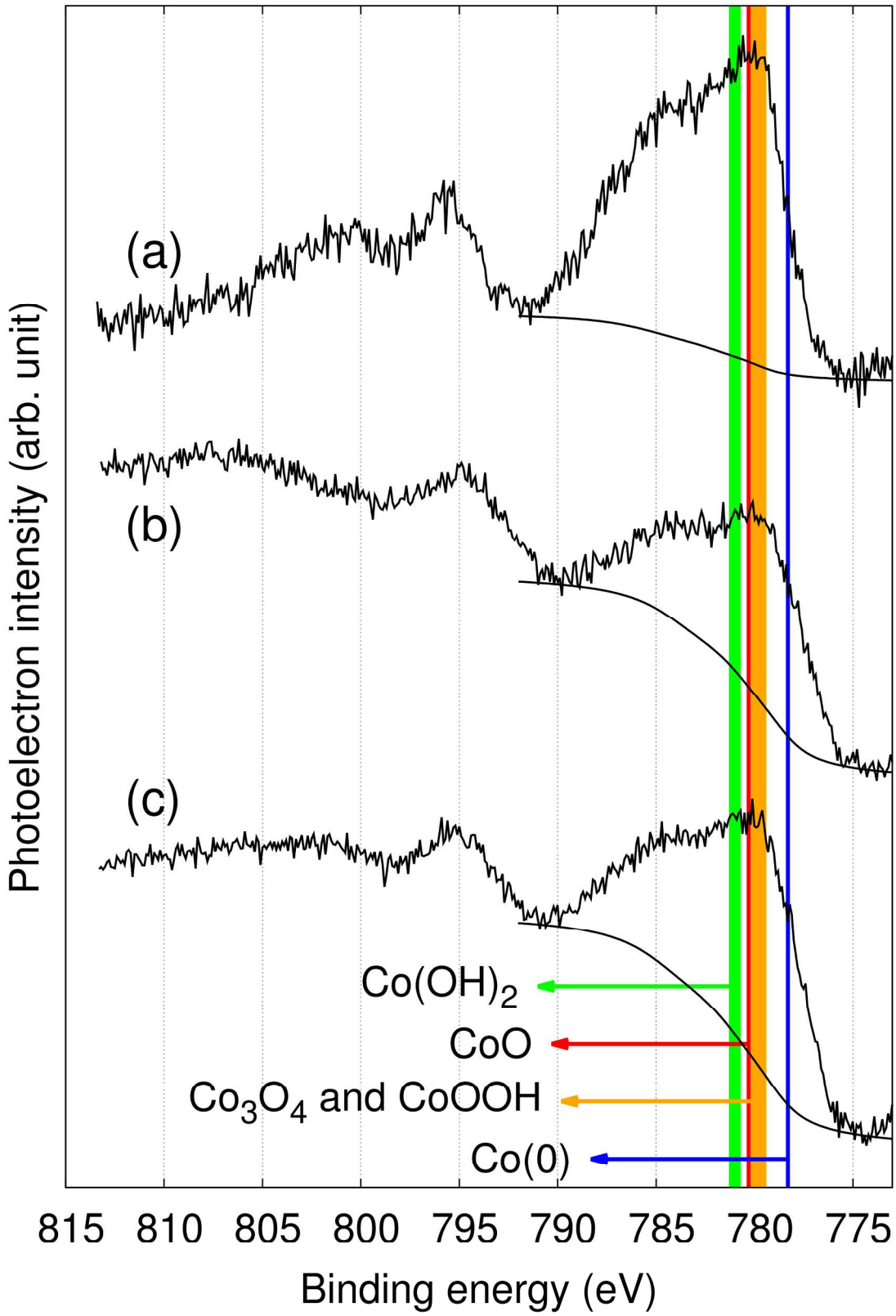

Fig. 7. XPS in Co 2p region for (a) ball-milled CoFe-CNFs, (b) CoFe-CNFs, and (c) Co-CNFs.

Conclusion

We developed a simple synthesis process of OER catalysts by carbonizing the electrospun polymer fibers mixed with Co or Fe-based precursors. CoFe-CNFs showed an OER performance comparable to Ir black catalyst and better performance was achieved than Co-CNFs containing the double amount of Co metal. From the surface characterizations with CV, we could observe that CoFe alloy shows different Co(III)/Co(II) redox peak of different potential, which might be related to the improved OER activity performance. In addition, the superior stability to Ir black catalyst is observed, likely due to the nanofibrous carbon envelopes surrounding metal nanoparticles. The carbon layers around nanoparticles are not so hindering the electrolyte contact to the active sites as intuitively expected but helpful to preserving catalyst surface in a highly oxidizing OER condition. Therefore, the developed CoFe-CNFs has a potential as bi-functional oxygen electrocatalysts applicable to metal-air battery or regenerative fuel cells under various potential conditions by utilizing the nanofibrous carbon structure not only as a support for homogeneous dispersion of the catalysts, but also as a protective envelope for enhancing the catalyst stability.

Acknowlegement

This work is also supported by the Core Technology Development Program of the Research Institute for Solar and Sustainable Energies (RISE), Gwangju Institute of Science and Technology. J. Lee is deeply indebted to the Alexander von Humboldt Foundation fellowship for experienced researchers (1141065).

References

1. D. K. Kinoshita, *Electrochemical Oxygen Technology*, Wiley-Interscience, 1st edn., 1992.
2. S. Trasatti, *J. Electroanal. Chem.*, 1980, **111**, 125–131.
3. S. Trasatti, *Electrochim. Acta*, 1984, **29**, 1503–1512.
4. H. Beer, 147AD.
5. S. Trasatti, *Electrochim. Acta*, 2000, **45**, 2377–2385.
6. M. E. G. Lyons and M. P. Brandon, *J. Electroanal. Chem.*, 2010, **641**, 119–130.
7. S. M. Jasem and A. C. C. Tseung, *J. Electrochem. Soc.*, 1979, **126**, 1353–1360.
8. R. D. L. Smith, M. S. Prévot, R. D. Fagan, S. Trudel, and C. P. Berlinguette, *J. Am. Chem. Soc.*, 2013, **135**, 11580–11586.
9. R. D. L. Smith, M. S. Prévot, R. D. Fagan, Z. Zhang, P. A. Sedach, M. K. J. Siu, S. Trudel, and C. P. Berlinguette, *Science*, 2013, **340**, 60–63.
10. Y. Li, W. Zhou, H. Wang, L. Xie, Y. Liang, F. Wei, J.-C. Idrobo, S. J. Pennycook, and H. Dai, *Nat. Nanotechnol.*, 2012, **7**, 394–400.
11. M. Gong, Y. Li, H. Wang, Y. Liang, J. Z. Wu, J. Zhou, J. Wang, T. Regier, F. Wei, and H. Dai, *J. Am. Chem. Soc.*, 2013, **135**, 8452–8455.
12. Y. Liang, Y. Li, H. Wang, J. Zhou, J. Wang, T. Regier, and H. Dai, *Nat. Mater.*, 2011, **10**, 780–786.
13. K. Mette, A. Bergmann, J.-P. Tessonnier, M. Hävecker, L. Yao, T. Ressler, R. Schlögl, P. Strasser, and M. Behrens, *ChemCatChem*, 2012, **4**, 851–862.
14. R. L. Doyle, I. J. Godwin, M. P. Brandon, and M. E. G. Lyons, *Phys. Chem. Chem. Phys.*, 2013, **15**, 13737–13783.
15. S. Uhm, B. Jeong, and J. Lee, *Electrochim. Acta*, 2011, **56**, 9186–9190.

16. D. Shin, B. Jeong, B. S. Mun, H. Jeon, H.-J. Shin, J. Baik, and J. Lee, *J. Phys. Chem. C*, 2013, **117**, 11619–11624.

17. B. Jeong, S. Uhm, and J. Lee, *ECS Trans.*, 2010, **33**, 1757–1767.

18. J. Lee, B. Jeong, and J. D. Ocon, *Curr. Appl. Phys.*, 2013, **13**, 309–321.

19. N. A. M. Barakat, B. Kim, S. J. Park, Y. Jo, M.-H. Jung, and H. Y. Kim, *J. Mater. Chem.*, 2009, **19**, 7371.

20. C. . Abreu, M. . Cristóbal, X. . Nóvoa, G. Pena, M. . Pérez, and C. Serra, *Electrochim Acta*, 2004, **49**, 3057–3065.

21. B. T. Hang, T. Watanabe, M. Eashira, S. Okada, J. Yamaki, S. Hata, S.-H. Yoon, and I. Mochida, *J. Power Sources*, 2005, **150**, 261–271.

22. A. Foelske and H.-H. Strehblow, *Surf. Interface Anal.*, 2002, **34**, 125–129.

23. D. Deng, L. Yu, X. Chen, G. Wang, L. Jin, X. Pan, J. Deng, G. Sun, and X. Bao, *Angew. Chem. Int. Ed.*, 2013, **52**, 371–375.

24. US. Pat., 6 127 060J. A. Read, 2000.

25. M. N. Golovin and I. Kuznetsov, 2000.

26. M. C. Biesinger, B. P. Payne, A. P. Grosvenor, L. W. M. Lau, A. R. Gerson, and R. S. C. Smart, *Appl. Surf. Sci.*, 2011, **257**, 2717–2730.

27. J. Yang, H. Liu, W. N. Martens, and R. L. Frost, *J. Phys. Chem. C*, 2010, **114**, 111–119.